Science
AAAS

Switchable Ferroelectric Diode and Photovoltaic Effect in BiFeO 3
T. Choi, *et al.*
Science **324**, 63 (2009);
DOI: 10.1126/science.1168636

Science (print ISSN 0036-8075; online ISSN 1095-9203) is published weekly, except the last week in December, by the American Association for the Advancement of Science, 1200 New York Avenue NW, Washington, DC 20005.

down the chondrogenic pathway in response to the microenvironment modification (Fig. 3C and fig. S5). To examine cell interaction with this dynamic microenvironment, fixed sections were immunostained for the expression of the $\alpha_v\beta_3$ integrin, one of the cell surface integrins by which cells interact with RGDS. Cells persistently presented with RGDS express the integrin, whereas most cells with RGDS photoreleased cease integrin expression by day 21 (Fig. 4A), indicating that the cells have locally sensed and responded to the chemical change in their environment. Additionally, to determine that the elevated GAG production is associated with chondrogenesis, sections of the cell-hydrogel constructs were immunostained for the hMSC marker CD105 (transforming growth factor–β receptor) and the chondrocyte marker COLII. As hMSCs differentiate into chondrocytes in 3D culture, a decrease in CD105 expression is observed along with onset of COLII production (*35*). The photolytic removal of RGDS on day 10 is accompanied by a decrease in CD105 expression and elevated COLII production as compared with persistently presented RGDS on day 21 (Fig. 4B), indicating increased chondrogenesis. With this photodegradable tether approach, the dynamic influence of other biomolecules on cell function can be similarly studied, expanding the ability to fabricate material environments that control cell function. Although manipulation of a single signal was examined and used to direct hMSC differentiation herein, this gel system can be readily functionalized with photolabile moieties of different light absorbances and cleavage efficiencies, enabling independent control over multiple signals through selection of irradiation wavelength and intensity.

We have demonstrated the synthesis of photodegradable macromers and their subsequent polymerization to form hydrogels whose physical, chemical, and biological properties can be tuned in situ and in the presence of cells by ultraviolet, visible, or two-photon irradiation. These photodegradable hydrogels show promise as in vitro 3D cell culture platforms in which cell-material interactions are dynamically and externally directed to elucidate how cells receive and process information from their environments. Ways to promote or suppress desired cell functions may become possible with temporal and spatial regulation of the 3D culture microenvironment, leading to applications in fields ranging from controlled drug delivery to tissue regeneration.

References and Notes

1. D. B. Weibel, W. R. DiLuzio, G. M. Whitesides, *Nat. Rev. Microbiol.* **5**, 209 (2007).
2. M. P. Lutolf, J. A. Hubbell, *Nat. Biotechnol.* **23**, 47 (2005).
3. R. Langer, N. A. Peppas, *AIChE J.* **49**, 2990 (2003).
4. M. M. Stevens, J. H. George, *Science* **310**, 1135 (2005).
5. G. Chan, D. J. Mooney, *Trends Biotechnol.* **26**, 382 (2008).
6. A. J. Engler, S. Sen, H. L. Sweeney, D. E. Discher, *Cell* **126**, 677 (2006).
7. A. J. Engler *et al.*, *J. Cell Biol.* **166**, 877 (2004).
8. P. A. Kenny, M. J. Bissell, *Int. J. Cancer* **107**, 688 (2003).
9. A. Metters, J. Hubbell, *Biomacromolecules* **6**, 290 (2005).
10. M. A. Rice, J. Sanchez-Adams, K. S. Anseth, *Biomacromolecules* **7**, 1968 (2006).
11. D. Seliktar, A. H. Zisch, M. P. Lutolf, J. L. Wrana, J. A. Hubbell, *J. Biomed. Mater. Res. Part A* **68A**, 704 (2004).
12. M. Ehrbar *et al.*, *Circ. Res.* **94**, 1124 (2004).
13. G. A. Silva *et al.*, *Science* **303**, 1352 (2004).
14. A. Khademhosseini, R. Langer, *Biomaterials* **28**, 5087 (2007).
15. R. W. Sands, D. J. Mooney, *Curr. Opin. Biotechnol.* **18**, 448 (2007).
16. M. S. Hahn, J. S. Miller, J. L. West, *Adv. Mater.* **18**, 2679 (2006).
17. J. H. Wosnick, M. S. Shoichet, *Chem. Mater.* **20**, 55 (2008).
18. Y. R. Zhao *et al.*, *J. Am. Chem. Soc.* **126**, 4653 (2004).
19. M. Alvarez *et al.*, *Adv. Mater.* **20**, 4563 (2008).
20. Y. Luo, M. S. Shoichet, *Nat. Mater.* **3**, 249 (2004).
21. S. A. Khan, I. M. Plitz, R. A. Frantz, *Rheol. Acta* **31**, 151 (1992).
22. R. J. Young, P. A. Lovell, *Introduction to Polymers* (Chapman & Hall, London, ed. 2, 1991).
23. S. J. Bryant, K. S. Anseth, in *Scaffolding in Tissue Engineering*, P. X. Ma, J. Elisseeff, Eds. (Marcel Dekker, New York, 2005), pp. 69–88.
24. S. J. Bryant, C. R. Nuttelman, K. S. Anseth, *J. Biomater. Sci. Polym. Ed.* **11**, 439 (2000).
25. P. Tayalia, C. R. Mendonca, T. Baldacchini, D. J. Mooney, E. Mazur, *Adv. Mater.* **20**, 4494 (2008).
26. G. P. Raeber, M. P. Lutolf, J. A. Hubbell, *Biophys. J.* **89**, 1374 (2005).
27. M. J. Mahoney, K. S. Anseth, *Biomaterials* **27**, 2265 (2006).
28. E. Ruoslahti, M. D. Pierschbacher, *Science* **238**, 491 (1987).
29. T. Boontheekul, D. J. Mooney, *Curr. Opin. Biotechnol.* **14**, 559 (2003).
30. G. A. Hudalla, T. S. Eng, W. L. Murphy, *Biomacromolecules* **9**, 842 (2008).
31. S. Tavella *et al.*, *J. Cell Sci.* **110**, 2261 (1997).
32. C. R. Nuttelman, M. C. Tripodi, K. S. Anseth, *Matrix Biol.* **24**, 208 (2005).
33. C. N. Salinas, K. S. Anseth, *Biomaterials* **29**, 2370 (2008).
34. A. M. DeLise, L. Fischer, R. S. Tuan, *Osteoarthritis Cartilage* **8**, 309 (2000).
35. C. N. Salinas, B. B. Cole, A. M. Kasko, K. S. Anseth, *Tissue Eng.* **13**, 1025 (2007).

36. The authors thank C. Bowman, T. Scott, and C. Kloxin for comments on early versions of this manuscript and valuable discussions; A. Aimetti for peptide synthesis training; J. McCall and S. Anderson for cell culture assistance; M. Schwartz for cell migration discussions; C. Bowman and his laboratory for use of and assistance with the rheometer and profilometer; C. Kloxin for assistance with image analysis; C. DeForest, Carl Zeiss, Inc., and the Howard Hughes Medical Institute Janelia Farms campus for assistance with and use of the Zeiss 710 two-photon confocal LSM; and the Howard Hughes Medical Institute and the NIH (grants DE12998 and DE16523) for research support. A.K. thanks the NASA Graduate Student Researchers Program fellowship and the Department of Education Graduate Assistance in Areas of National Need fellowship for support. A patent related to this work has been submitted (U.S. Patent Application No. 11/374,471).

Supporting Online Material

www.sciencemag.org/cgi/content/full/324/5923/59/DC1
Materials and Methods
SOM Text
Figs. S1 to S5
References

8 December 2008; accepted 3 February 2009
10.1126/science.1169494

Switchable Ferroelectric Diode and Photovoltaic Effect in $BiFeO_3$

T. Choi, S. Lee,* Y. J. Choi, V. Kiryukhin, S.-W. Cheong†

Unidirectional electric current flow, such as that found in a diode, is essential for modern electronics. It usually occurs at asymmetric interfaces such as p-n junctions or metal/semiconductor interfaces with Schottky barriers. We report on a diode effect associated with the direction of bulk electric polarization in $BiFeO_3$: a ferroelectric with a small optical gap edge of ~2.2 electron volts. We found that bulk electric conduction in ferroelectric monodomain $BiFeO_3$ crystals is highly nonlinear and unidirectional. This diode effect switches its direction when the electric polarization is flipped by an external voltage. A substantial visible-light photovoltaic effect is observed in $BiFeO_3$ diode structures. These results should improve understanding of charge conduction mechanisms in leaky ferroelectrics and advance the design of switchable devices combining ferroelectric, electronic, and optical functionalities.

Ferroelectrics undergo a transition from a high-symmetry structure to a low-symmetry state with a spontaneous electric polarization below a transition temperature. They usually consist of a complex microstructure of domains with different orientations of the polarization that can be switched with external electric fields (*1*). Ferroelectrics are typically highly insulating because of large band gaps (*2*), and any current leakage has been considered to be a serious problem that deteriorates their functionalities (*3*, *4*). The relationship between electronic transport characteristics and ferroelectric polarization has been little studied. This is partially due to complexity associated with ferroelectric domains. In addition, leakage often occurs through extended crystallographic defects such as grain boundaries or ferroelectric domain boundaries, so the true bulk leakage conduction may not be always dominant.

Rutgers Center for Emergent Materials and Department of Physics and Astronomy, Rutgers University, Piscataway, NJ 08854, USA.

*Present address: Neutron Science Division, Korea Atomic Energy Research Institute, Daejeon 305-353, Korea.
†To whom correspondence should be addressed. E-mail: sangc@physics.rutgers.edu

On the other hand, bulk photocurrent can be induced by high-energy light illumination even in good insulators; and directional photocurrent without external bias [that is, a photovoltaic (PV) effect] has been studied in ferroelectrics (*5*–*13*). When a ferroelectric in an open circuit is illuminated by ultraviolet light, for example, a high photovoltage, much larger than the band gap, has been observed in the direction of the electric polarization (*5*–*8*). The magnitude of this photovoltage is directly proportional to the crystal length in the polarization direction. In addition, a steady-state photocurrent can be generated in the direction of electric polarization when a ferroelectric under continuous light illumination forms a closed circuit. This PV effect in ferroelectrics is distinctly different from the typical PV effect in semiconductor p-n junctions, and was investigated in Pb-based ferroelectric oxides (*9*–*11*) and $LiNbO_3$ (*6*, *8*). However, the observed photocurrent density turns out to be minuscule—on the order of a few nanoamperes/cm^2, mainly due to poor bulk dc conduction of the ferroelectrics (*8*, *9*, *11*). Utilization of small–optical-gap ferroelectrics with good carrier transport properties and large absorption of visible light extending into the red range is therefore a promising route toward novel optoelectronic applications. It may, for example, lead to increased power conversion efficiency in solar energy applications. The origin of the PV effect in ferroelectrics is controversial and has been discussed in terms of extrinsic effects such as the excitation of electrons from asymmetric impurity potentials (*12*), interfacial effects due to polarization-dependent band bending at metal-ferroelectric interfaces (*9*), or intrinsic effects such as asymmetric induced polarization through nonlinear optical processes (*13*–*15*).

Ferroelectric $BiFeO_3$ (BFO) contains transition metal ions with unpaired *d* electrons. The presence of the *d* electrons can result in a relatively small optical gap and give rise to a high concentration of charged impurities and defects (*16*). BFO becomes ferroelectric at a critical temperature (T_c) ≈ 1100 K, below which BFO exhibits a rhombohedral *R*3*c* structure with a perovskite pseudocubic unit cell (a ≈ 3.96 Å, α ≈ 89.4°) elongated along the [111] direction that coincides with the electric polarization vector ***P***. Each of our BFO crystals contained a single ferroelectric domain (*17*, *18*). Here we describe the electronic transport properties of three thin platelike BFO crystals placed between symmetric electrodes: BFO1 (~70 μm thickness, ~2 × 2 mm^2 in-plane dimension, and ~0.6-mm-diameter circular thick Au electrodes), BFO2 (~80 μm thickness, ~2.5 × 2.5 mm^2 in-plane dimension, and ~1.6 × 1 mm^2 semitransparent Au electrodes), and BFO3 (~90 μm thickness, ~1 × 2 mm^2 in-plane dimension, and ~0.6-mm-diameter circular thick Ag or Au electrodes). The BFO plates are normal to a principal axis of the pseudocubic cell, and the "in-plane or out-of-plane" component of the polarization is defined with respect to the plate surface.

We found that in all investigated specimens, there existed substantial currents that were nonlinear with applied electric field E and also depended strongly on the direction of E. The magnitude of E here is much less than ferroelectric coercivity (fig. S1), so polarization switching does not occur during the E sweep for current density, J, versus E curves. Figure 1A shows linear-scale $J(E)$ curves of BFO1 at 300 and 350 K, which exhibit diodelike behavior. For the typical p-n junction diodes, the forward current density follows an exponential relationship with applied voltage given by $J \propto \exp(qV/\alpha k_B T)$, where q is the electron charge, V is voltage, α is a constant called the ideality factor, and k_B is the Boltzmann constant. In the range of 0.05 to 0.15 kV/cm forward bias, α is 6.3 at 300 K and 4.7 at 350 K. This large ideality factor, much larger than the ideal value of 1 in semiconductor p-n junctions, has been observed in perovskite-based oxide p-n junctions, where charge trapping at defects in the bulk seems important for transport properties (*19*). We also found that J increases drastically with increasing temperature from 200 to 350 K as evident in the semi-log plot of $J(E)$ curves in the inset of Fig. 1A. In addition, the asymmetry in the $J(E)$ curve also increases with increasing T. The rectification ratios, defined as the ratios of the positive current divided by the negative one for E = ±1.3 kV/cm, at 200, 250, 300, and 350 K, are 13, 159, 488, and 495, respectively.

The diode forward and reverse directions switch when ferroelectric polarization is uniformly reversed by large electric voltage pulses. When +150-V (an E of +17 kV/cm) pulses are applied to the top electrode of BFO3 shown in Fig. 2A, the ferroelectric polarization points down, as confirmed by piezoresponse force microscopy (PFM; see supporting online materials and methods) (Fig. 2B). The electric current through the specimen is large when the current direction is also downward; that is, the diode forward direction is from top to bottom, and along the polarization direction (Fig. 2C). When –150-V pulses are applied, ferroelectric polarization switches to the upward direction, and the diode forward direction becomes from bottom to top (still along the polarization direction). Application of +150-V pulses restores the original configuration. Therefore, the diode directions switch whenever ferroelectric polarization is reversed by external pulses, and the diode forward direction is always along the ferroelectric polarization direction (Fig. 2C). The application of the second set of +150-V pulses does not completely restore the original $J(E)$ curve, and this incomplete restoration may be due to complex factors such as incomplete polarization flipping, the formation of conducting paths, or irreversible changes in the interfacial

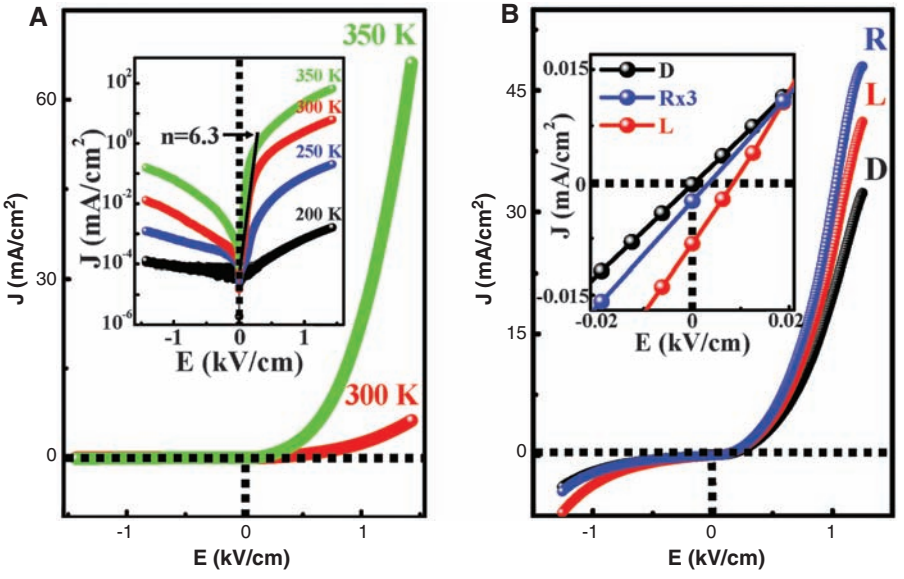

Fig. 1. (**A**) $J(E)$ curve of a symmetric Au/BFO1/Au structure in the dark at 300 and 350 K. A substantial diodelike effect is evident. The inset shows semi–log-scale $J(E)$ curves at various temperatures. All $J(E)$ measurements were performed by sweeping the voltage from the positive maximum to the negative maximum in vacuum at 200 to 350 K. The applied electric fields are far below the coercive field for polarization switching. (**B**) $J(E)$ curves of the BFO2 sample in the dark (D) and with green-light illumination on right (R) or left (L) semitransparent Au electrodes. Current for either E direction (except very near E = 0) increases with illumination on either side. The inset shows an expanded view of the $J(E)$ curves near zero bias field (E = 0). Zero-bias current flows along the reverse direction with illumination from either direction: Left-side illumination works better than right-side illumination for this particular setup, and the x and y axes for the right-side illumination are expanded by a factor of 3 to clearly show the presence of the reverse-direction current at zero bias.

regions. In the above discussion, we consider only the out-of-plane component of ferroelectric polarization because of the platelike geometry of the Ag/BFO3/Ag structure. We emphasize that even though the simultaneous $J(E)$ and PFM experiments with electric pulses were performed only on BFO3, the switchable $J(E)$ curves were observed in all specimens that we have investigated.

The observed diodelike behavior of dc conduction implies a possibility of zero-bias PV effect in BFO. Because the optical gap edge of BFO is reported to be ~2.2 eV (*20*), visible light is expected to induce substantial photocurrent. We, in fact, found a substantial PV effect in BFO with semitransparent Au electrodes illuminated with visible light [wavelength (λ) = 532-nm green light and λ = 630-nm red light], with the total power density being less than 20 mW/cm^2.

Figure 1B depicts the $J(E)$ curves of BFO2 with symmetric Au electrodes in green light as well as in the dark. Green light illuminated either left or right semitransparent Au electrodes of BFO2 (see the experimental schematic in the inset of Fig. 3). Illumination on either side induces the increase of conductance with the direction of photocurrent after the direction of the external bias. In other words, measurable photoconduction occurs with illumination. At zero bias, the photocurrent also exists and is always negative, independent from the illumination direction: negative 0.13 μA, corresponding to reverse bias direction 8.219 μA/cm^2 for the BFO2 configuration with left-side illumination; and 0.013 μA, corresponding to reverse bias direction 0.849 μA/cm^2 for the configuration with right-side illumination (Fig. 1B, inset). This bulk photocurrent in the absence of an external bias indicates that charge carriers induced by light illumination move preferentially along one direction; that is, there is a PV effect in BFO2. Figure 3 shows the time dependence of the photocurrent at zero bias in BFO2 with the turning of a green (top panel) and a red (bottom panel) light on and off. For the first 60 min, the left electrode was illuminated and for the next 60 min the right electrode was illuminated. Photoconductivity was reported in ferroelectric monodomain (111) BFO films, but any PV effect (nonzero photoconductivity at zero bias) was not discussed in the report (*21*).

In principle, thermal variation induced by visible-light illumination can contribute to the photocurrent increase shown in Fig. 1B, but the decrease of resistance due to a light-induced temperature increase cannot cause the observed negative steady photocurrent at zero bias. On the other hand, a pyroelectric current can be generated by the change of the magnitude of ferroelectric polarization because of the temperature increase caused by light illumination. However, this is a transient effect that occurs while the temperature is changing, and no steady-state photocurrent is expected from the pyroelectric effect. Thus, although the initial small spikes of photocurrent in Fig. 3 can be attributed to the pyroelectric effect, the steady-state photocurrent in Fig. 3 has a different origin. Consistently, when the light is switched on, the photocurrent increases suddenly to a transient maximum before reaching a steady state. The transient component with green light is ~6% of the steady-state photocurrent, and the time constant associated with the transient component is ~15 s. The transient component with red light is ~25% of the steady-state photocurrent and the time constant is ~60 s. The steady-state photocurrent density is ~7.35 μA/cm^2 under green light illumination on the left side. This value is much larger than the 2.6 nA/cm^2 observed under red light illumination, indicating that the photoexcited charge carriers across the bulk optical gap of ~2.5 eV contribute to the PV effect in BFO. Finally, because our BFO crystals are conducting, an equilibrium temperature gradient generated by continuous light illumination on one side of BFO can produce a steady current due to thermoelectric power voltage. However, this effect should produce an opposite-direction current when the light-illumination direction is changed from one side to the other of the BFO crystal. Our zero-bias photocurrent direction is always fixed, independent of the light-illumination conditions, which is inconsistent with the thermoelectric power scenario. On the other hand, the thermoelectric power effect may contribute to the asymmetry in the magnitude of the photocurrent with different-side light illumination, which turns out to be substantial in BFO2. Obviously, any uncontrolled asymmetry in the electrode configuration or light-illumination conditions can also contribute to the left-right asymmetry in the magnitude of the photocurrent.

A linear polarizer was placed between the light source and BFO2 to measure the effect of light polarization on the PV effect (Fig. 4, inset). The angle θ between the in-plane component of ferroelectric polarization (determined by in-plane PFM) and the electric field vector of linearly polarized light was varied by 360°. The change of the photocurrent at zero bias with θ, shown in Fig. 4 with blue circles, closely follows a sinusoidal form with a periodicity of 180°. The maximum of photocurrent was observed when the polarized-light electric field was along the in-plane ferroelectric polarization, and the current was minimal when the light electric field was perpendicular to the in-plane ferroelectric polarization. After the initial rotation experiment, the polarizer was rotated by 90°, and lighting conditions were readjusted for an optimum photocurrent. The change of photocurrent (green circles) with θ after this polarizer rotation is similar to the one before rotating the polarizer, except for a 90° phase shift of θ. This demonstrates that the reproducible angular dependence is not due to any artifact of our optical setup.

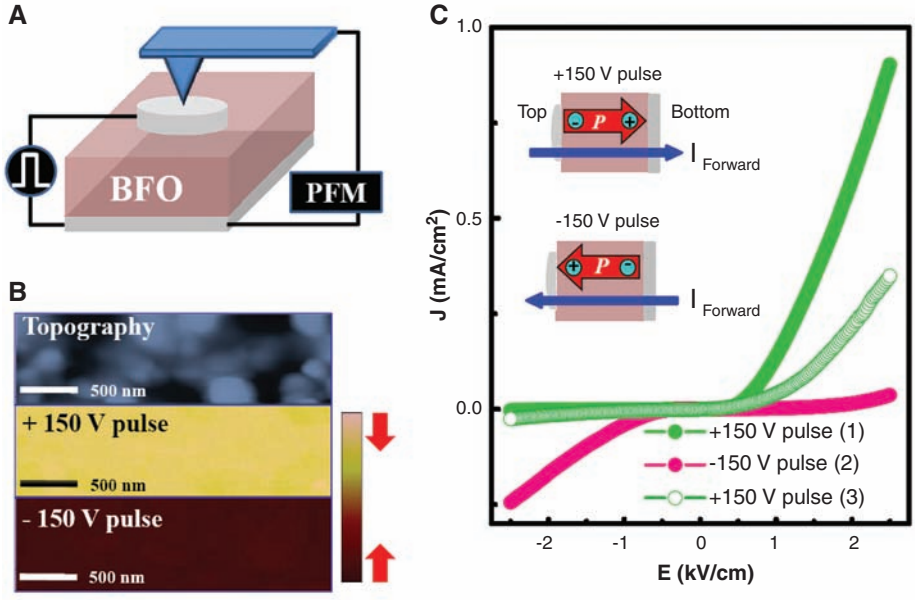

Fig. 2. (**A**) Sketch of the setup for the simultaneous PFM and $J(E)$ measurements on Ag/BFO3/Ag. One hundred electric pulses with ±150 V (E = 17 kV/cm) and a duration of 0.01 s were used to flip electric polarization. $J(E)$ was measured up to E = 2.5 kV/cm, and ac voltage of 1 V_{rms} and 17 kHz was used for PFM. (**B**) Topography image and out-of-plane PFM images after ±150-V pulses. The PFM signal is color-scaled. These images show that +150-V pulses induce a homogeneous state with downward out-of-plane polarization, and −150-V pulses induce a homogeneous state with upward polarization. (**C**) $J(E)$ curves of BFO3 after +150-V, −150-V. and +150-V pulses, in sequence. The diode forward and reverse directions switch when the direction of out-of-plane polarization (P) is reversed by ±150-V pulses. The diode forward direction turns out to be the same as the direction of electric pulses used for polarization flipping.

The above observations shed light on the origin of the PV effect in BFO. The sinusoidal behavior of the photocurrent at zero bias observed in the polarized-light rotation experiment is consistent with a nonlinear optical effect scenario (*13*). When a ferroelectric is under intense light illumination, the second-order optical response combined with a linear term is well known to induce an asymmetric polarization, which can result in an optical rectification effect (*14*, *15*). It was proposed that the asymmetric induced polarization can also give rise to a dc rectification-like effect such as a PV effect. This effect is supposed to be maximal when the polarized-light electric field is along the ferroelectric polarization and follows a sinusoidal angular dependence. This second-order optical response is an intrinsic bulk effect, and therefore it should not be sample-dependent. However, we found a noticeable variation in the magnitude of the rectification and PV effects in different samples, suggesting the importance of impurities and defects with respect to the transport mechanism. The space charge–limited conduction suggested in the diode behavior (figs. S2 and S3) is also consistent with the importance of impurities and defects. Any polarization-related asymmetry of impurity potentials can render the photocurrent sensitive to the orientation of light polarization, probably in a sinusoidal manner (*12*). Simple polarization-dependent band-bending at the metal/BFO interfaces probably does not produce the observed directional dependence. In addition, we found little difference between the effects of Ag and Au electrodes on the diode effect (fig. S4), suggesting no major contribution from the band-bending at the metal/BFO interfaces. On the other hand, the contribution of impurities and defects coupled with the band-bending or the second-order optical response to photocurrent can be influenced by the orientation of polarization.

We report here that single–ferroelectric-domain BFO crystals exhibit a diodelike effect. The forward direction of the diode is determined by the direction of the electric polarization, and the directionality of the diode can be reproducibly switched by large external electric fields. Associated with the diode effect, a substantial zero-bias PV current is induced by visible light. Further study of these effects, such as experiments involving electrodes with different conductors or controlled doping levels and spectroscopic studies of metal/BFO interfaces, will be necessary to unveil their true origin. The observation of switchable diode and photovoltaic effects in BFO reveals unusual and intriguing charge conduction behavior in leaky ferroelectrics, and should advance studies of BFO-based multifunctional devices.

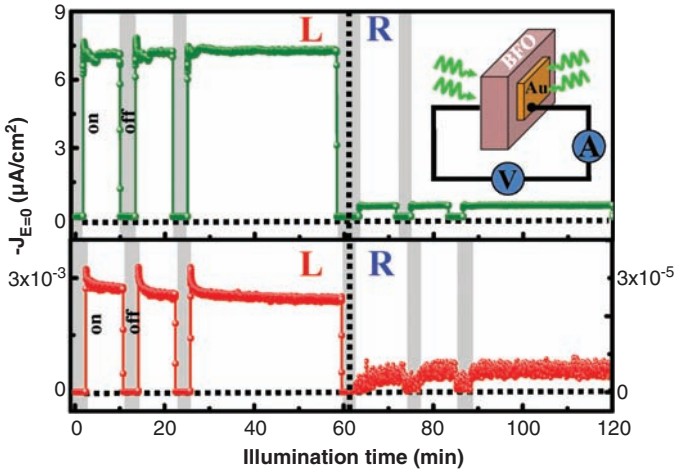

Fig. 3. The zero-bias photocurrent density as a function of time with (**top**) green light (λ = 532 nm) or (**bottom**) red light (λ = 650 nm) on or off, shining on the different sides of BFO2 (a sketch is shown in the inset). The total light power was <3 mW, and the short-circuit photocurrent was measured every 100 ms. The current with the light off decreased to <~0.1 pA. Illumination from either side results in the same-direction zero-bias photocurrent, unambiguously demonstrating the PV effect in ferroelectric BFO. The large difference in the magnitude of photocurrent between green- and red-light illumination indicates that photoexcited carriers across the bulk optical gap (~2.5 eV) dominate the PV effect. The observed right-left asymmetry may result from a thermoelectric power effect and/or uncontrolled asymmetries in the experimental configuration.

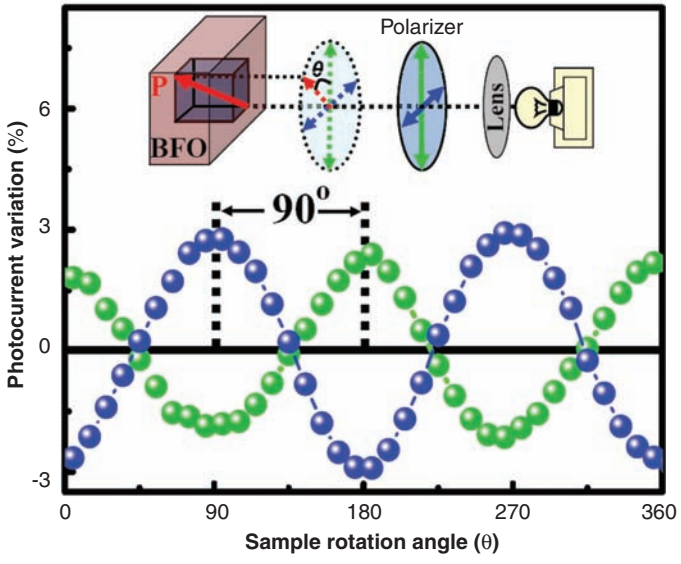

Fig. 4. The variation of photocurrent with sample rotation under illumination with a linearly polarized light. The experimental sketch is shown in the inset. The PV effect becomes maximum when the polarized-light electric field is parallel to the in-plane component of the ferroelectric polarization, and minimum when the field is perpendicular to the in-plane component.

References and Notes

1. J. F. Scott, *Ferroelectric Memories* (Springer, Heidelberg, Germany, 2000).
2. M. Dawber, K. M. Rabe, J. F. Scott, *Rev. Mod. Phys.* **77**, 1083 (2005).
3. J. F. Scott, *J. Phys. Condens. Matter* **20**, 021001 (2008).
4. J. Wang *et al.*, *Science* **299**, 1719 (2003).
5. V. M. Fridkin, B. N. Popov, *Sov. Phys. Usp.* **21**, 981 (1978).
6. A. M. Glass, D. Von der Linde, T. J. Negran, *Appl. Phys. Lett.* **25**, 233 (1974).
7. N. Noginova *et al.*, *J. Opt. Soc. Am. B* **14**, 1390 (1997).
8. G. Dalba, Y. Soldo, F. Rocca, V. M. Fridkin, Ph. Sainctavit, *Phys. Rev. Lett.* **74**, 988 (1995).
9. Y. S. Yang *et al.*, *Appl. Phys. Lett.* **76**, 774 (2000).
10. P. Poosanaas, A. Dogan, S. Thakoor, K. Uchino, *J. Appl. Phys.* **84**, 1508 (1998).
11. L. Pintilie, I. Vrejoiu, G. L. Rhun, M. Alexe, *J. Appl. Phys.* **101**, 064109 (2007).
12. V. I. Belinicher, B. I. Sturman, *Sov. Phys. Usp.* **23**, 199 (1980).
13. K. Tonooka, P. Poosanaas, K. Uchino, *Proc. SPIE* **3324**, 224 (1998).
14. M. Bass, P. A. Franken, J. F. Ward, G. Weinreich, *Phys. Rev. Lett.* **9**, 446 (1962).
15. A. Rice *et al.*, *Appl. Phys. Lett.* **64**, 1324 (1994).
16. A. J. Hauser *et al.*, *Appl. Phys. Lett.* **92**, 222901 (2008).
17. S. Lee, W. Ratcliff II, S.-W. Cheong, V. Kiryukhin, *Appl. Phys. Lett.* **92**, 192906 (2008).
18. S. Lee *et al.*, *Phys. Rev. B* **78**, 100101 (2008).
19. Y. W. Xie *et al.*, *J. Phys. Condens. Matter* **19**, 196223 (2007).
20. F. Gao *et al.*, *Appl. Phys. Lett.* **89**, 102506 (2006).
21. S. R. Basu *et al.*, *Appl. Phys. Lett.* **92**, 091905 (2008).

22. This work was funded by NSF (grants NSF-DMR-0804109 and 0704487). T.C. was partially supported by a Korea Research Foundation Grant funded by the Korean government (MOEHRD, grant KRF-2007-357-C00023).

Supporting Online Material

www.sciencemag.org/cgi/content/full/1168636/DC1
Materials and Methods
Figs. S1 to S4
References

17 November 2008; accepted 3 February 2009
Published online 19 February 2009;
10.1126/science.1168636
Include this information when citing this paper.